ACS APPLIED MATERIALS & INTERFACES

Research Article

www.acsami.org

Fabrication of Au@Ag Core/Shell Nanoparticles Decorated TiO_2 Hollow Structure for Efficient Light-Harvesting in Dye-Sensitized Solar Cells

Juyoung Yun, Sun Hye Hwang, and Jyongsik Jang*

School of Chemical and Biological Engineering, Seoul National University, 599 Gwanangno, Gwanakgu,, Seoul 151-742, Korea

Supporting Information

ABSTRACT: Improving the light-harvesting properties of photoanodes is promising way to enhance the power conversion efficiency (PCE) of dye-sensitized solar cells (DSSCs). We synthesized Au@Ag core/shell nanoparticles decorated TiO_2 hollow nanoparticles (Au@Ag/TiO_2 HNPs) via sol−gel reaction and chemical deposition. The Au@Ag/TiO_2 HNPs exhibited multifunctions from Au@Ag core/shell NPs (Au@Ag CSNPs) and TiO_2 hollow nanoparticles (TiO_2 HNPs). These Au@Ag CSNPs exhibited strong and broadened localized surface plasmon resonance (LSPR), together with a large specific surface area of 129 m^2 g^{-1}, light scattering effect, and facile oxidation−reduction reaction of electrolyte from TiO_2 HNPs, which resulted in enhancement of the light harvesting. The optimum PCE of η = 9.7% was achieved for the DSSCs using photoanode materials based on TiO_2 HNPs containing Au@Ag/TiO_2 HNPs (0.2 wt % Au@Ag CSNPs with respect to TiO_2 HNPs), which outperformed by 24% enhancement that of conventional photoanodes formed using P25 (η = 7.8%).

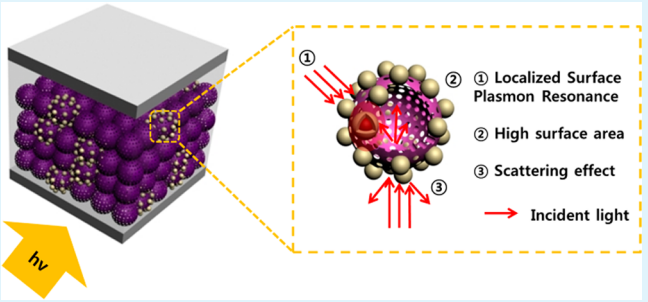

KEYWORDS: *TiO_2, hollow nanoparticles, metal core/shell nanoparticles, localized surface plasmon resonance, dye-sensitized solar cells*

INTRODUCTION

Dye-sensitized solar cells (DSSCs) have been the subject of much recent research interest due to the low costs, facile fabrication, and high power conversion efficiency (PCE).[1−3] In current systems, the dyes on a metal oxide absorb light in photoanode, generating electron−hole pairs and injecting electrons into the conduction band of the metal oxide. The dye is regenerated by electron transfer from an electrolyte, which is reduced at a counter electrode.[4,5] To improve the PCE, investigations into the properties of the photoanode have been carried out because of the importance of the photoanode for light harvesting and electron transfer. Methods to improve the PCE include increased light harvesting via localized surface plasmon resonance LSPR,[6−9] fluorescence resonance energy transfer based quantum dots (FRET-based QDs),[10,11] TiO_2 film with high surface area to enable sufficient dye loading,[12] spatial separation of cosensitization,[13] the use of light-scattering materials (LSMs),[14−16] rapid electron transfer via 1-dimensional metal oxides,[17−19] and the use of carbon-based materials.[20,21]

In particular, LSPR using metal nanoparticles has been used to improve light harvesting at the photoanode. The absorption intensity of LSPR, the plasmon bandwidth, and the stability of metal nanoparticles are important in determining the light-harvesting efficiency. Au and Ag nanoparticles have received much attention due to the excellent LSPR properties.[7,22] Au nanoparticles have advantages of favorable stability and facile synthesis, whereas the use of Ag nanoparticles leads to a larger extinction coefficient.[23] To control the LSPR properties, control over the size, morphology, and structure of the metal nanoparticles is required.[24,25] Particularly, proper control over the core/shell structure of Au and Ag in a single system can increase the absorption intensity, plasmon bandwidth, and stability.[26−28]

Light-scattering materials (LSMs) are an alternative approach to improving light harvesting due to a longer path length of the light and improved optical confinement in the photoanode. Micron-sized particles, nanofibers, and hollow particles have been applied in the light-scattering layer;[29−32] however, a single-material LSM has the disadvantage of low specific surface area, leading to insufficient dye loading and irregular packing in the photoanode owing to the micron scale. SiO_2/TiO_2 composite structures with a large specific surface area have been used to enhance the light-harvesting efficiency; however, they do not enable electron transfer between the materials owing to the insulating properties of SiO_2 and the SiO_2/TiO_2 composite structures has only light-scattering effects.[33] Therefore, LSMs with both a large specific surface area and efficient electron transfer properties are highly desirable.[31,34] To meet these requirements, we here propose the use of Au@Ag core/

Received: November 17, 2014
Accepted: January 6, 2015
Published: January 6, 2015

DOI: 10.1021/am508065n
ACS Appl. Mater. Interfaces 2015, 7, 2055−2063

shell nanoparticles decorated on TiO_2 hollow nanoparticles (HNPs). These structures can obtain strong LSPR, a large specific surface area, favorable optical scattering properties, and efficient electron transfer.

Herein, we successfully synthesized Au@Ag/TiO_2 HNPs, which have synergetic effects of enhanced absorption, broadened plasmon bandwidth, and favorable stability. Additionally, the TiO_2 HNPs have excellent properties for photoanode materials, with a Brunauer–Emmett–Teller (BET) specific surface area of 129 m^2 g^{-1} and strong optical scattering effects. Electron transfer is effective via intrashell charge transport in the TiO_2, which is composed of an anatase crystalline phase. We fabricated DSSCs based on Au@Ag/TiO_2 HNPs, which exhibited large PCE of η = 9.7%. To our knowledge, this is first demonstration of the photovoltaic application of Au@Ag/TiO_2 HNPs, providing enhanced LSPR via the synergistic effects of Au@Ag CSNPs, together with the large specific surface area and the favorable optical scattering properties of the TiO_2 HNPs.

RESULTS AND DISCUSSION

Fabrication of Au@Ag Core/Shell Nanoparticles Decorated TiO_2 Hollow Nanoparticles. Figure 1 shows an

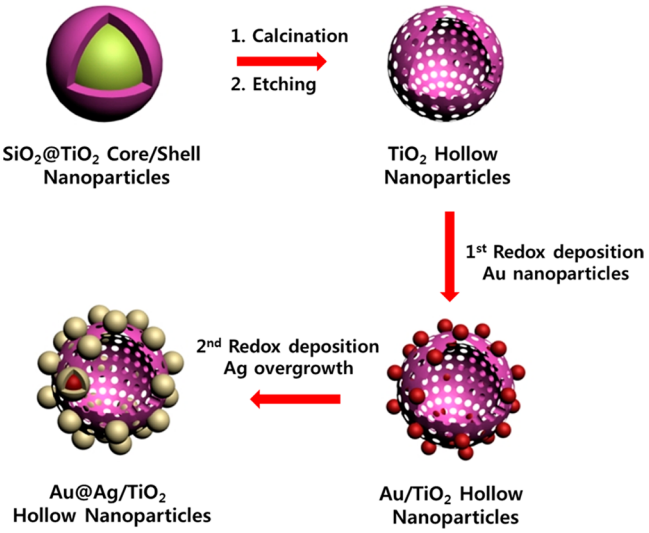

Figure 1. Schematic illustration of synthetic procedures of the Au@Ag/TiO_2 hollow nanoparticles.

illustration of the synthesis of the Au@Ag/TiO_2 HNPs. We have previously reported the synthesis of SiO_2@TiO_2 core/shell nanoparticles (CSNPs) using a sol–gel method.[35] The SiO_2@TiO_2 CSNPs, which had an amorphous TiO_2 shell, were transformed into anatase TiO_2 HNPs via calcination at 900 °C for 6 h, followed by selective etching of the SiO_2 core using aqueous NaOH solution. The surface of TiO_2 HNPs was then functionalized with a thiol group by using 3-mercaptopropyl trimethoxysilane (MPTS). The Au ions then were reduced and grown by a reducing agent at the surface of MPTS-treated TiO_2 HNPs via first redox deposition due to strong affinity between the sulfur in thiol group and metal atoms.[36] The reducing agent used was octyl amine (OA), in which the alkyl chain stabilizes the nucleation and growth of metal nanoparticles. The Ag shell can then be fabricated by coating with the Au nanoparticles via a second redox deposition. The surface of the Au seeds act as nucleation sites for the overgrowth of an Ag region, and the closely matched lattice constants enable a coating of Ag onto the surface of the Au nanoparticles.[37] Thus, an Ag shell can be overgrown on the Au nanoparticles epitaxially. Under the conditions described here, the thickness of the Ag shell can be tuned by controlling the amount of the Ag precursor.

Figure 2 displays transmission electron microscopy (TEM) images of the SiO_2@TiO_2 CSNPs, TiO_2 HNPs, and Au@Ag/

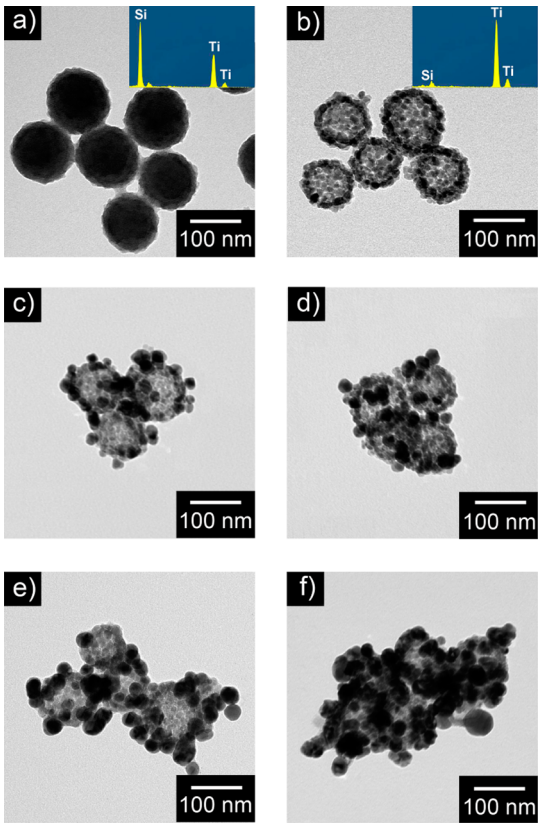

Figure 2. TEM images and EDS spectra of (a) SiO_2@TiO_2 CSNPs, (b) TiO_2 HNPs. (c–f) TEM images of Au@Ag/TiO_2 HNPs according to precursor ratio of Ag and Au (P_{Ag}/P_{Au} = 0.5, 1, 2, 4).

TiO_2 HNPs. Figure 2a shows that the SiO_2@TiO_2 CSNPs had an average diameter of 110 ± 10 nm. The diameter of the TiO_2 HNPs was 100 ± 10 nm, as shown in Figure 2b; these nanoparticles had undergone calcination and a selective etching process, and during the calcination, the SiO_2@TiO_2 CSNPs shrank because the amorphous TiO_2 shells were transformed into anatase TiO_2. The TiO_2 HNPs were therefore smaller than the SiO_2@TiO_2 CSNPs. The insets of Figure 2a,b show energy dispersive X-ray spectroscopy (EDS) data for the SiO_2@TiO_2 CSNPs and TiO_2 HNPs, respectively. The EDS analyses of the SiO_2@TiO_2 CSNPs and TiO_2 HNPs show that elemental composition of Si and Ti changed from 58:42 to 2:98 following calcination and etching, and it appears that almost the entire SiO_2 core had been removed during the etching process. Figure 2c–f show TEM images of Au@Ag/TiO_2 HNPs. The molar ratios of Ag and Au were 0.5:1, 1:1, 2:1, and 4:1, which we term here S1, S2, S3, and S4, respectively. The Au@Ag CSNPs were larger when the Ag fraction was larger. The Ag shell of the S4 nanoparticles exhibited significant aggregation during the second redox deposition step. Unlike others, in the case of S4, all Ag ions that were deposited during the second redox reaction cannot be reduced on the surface of the Au

DOI: 10.1021/am508065n
ACS Appl. Mater. Interfaces 2015, 7, 2055–2063

nanoparticles; hence, aggregation and side reaction occurred. With the S4 nanoparticles, Au@Ag CSNPs were not fabricated efficiently due to the loss of the Ag precursor which can be confirmed by yellow sol in the centrifuged solution. Au and Ag nanoparticles can also be decorated onto the surface of the TiO_2 HNPs separately. As a control for the S3/TiO_2 HNPs, the same amounts of Au and Ag precursor were reduced directly onto the surface of the TiO_2 HNPs separately. TEM images of the resulting Au/TiO_2 HNPs and Ag/TiO_2 HNPs show that Au nanocrystals of 15 ± 5 nm and Ag nanocrystals of 25 ± 5 nm diameter formed at the surface of the TiO_2 HNPs in Supporting Information, Figure S1.

Figure 3a–d show high-resolution TEM (HR-TEM) images of the nanoparticles S1–S4. These images indicate a core/shell

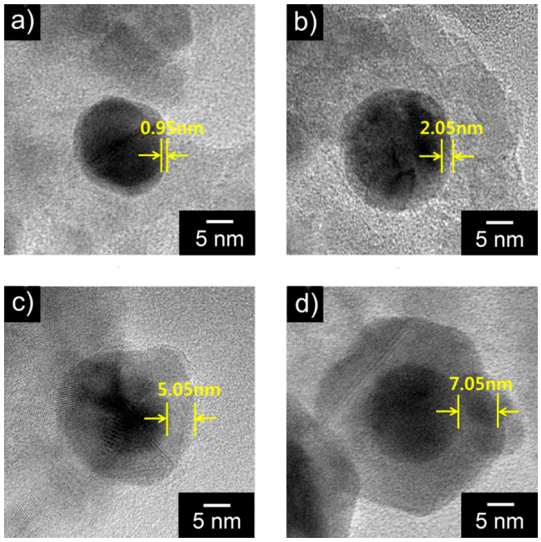

Figure 3. HR-TEM images of Au@Ag CSNPs decorated on the surface of TiO_2 HNPs with Ag shell thickness of (a) 0.95 nm, (b) 2.05 nm, (c) 5.05 nm, and (d) 7.05 nm.

structure of the Au@Ag CSNPs, which had Au seeds with an average diameter of 15 ± 5 nm. The Ag shell can be distinguished from the Au core in the images, appearing brighter than the Au core in HR-TEM. The thickness of the Ag shell increased as the ratio of Ag precursor to Au precursor increased. However, in the case of S4, the thickness of the Ag shell was not proportional to the amount of Ag precursor in S4, which is attributed to loss of the Ag precursor.

To investigate the elemental distribution of Au@Ag CSNPs, electron energy-loss spectroscopy (EELS) dot mapping and scanning TEM/EDS (STEM-EDS) line analysis is shown in Figure 4. The EELS dot mapping (Figure 4a–d) confirms the existence of Ag shells in the Au@Ag CSNPs. The STEM-EDS line analysis shown in Figure 4e–h indicates that the Au@Ag CSNPs have Au cores and Ag shells. The thickness of the Ag shell in these data is consistent with the HR-TEM analyses. The EDS analysis of Au@Ag/TiO_2 HNPs verifies the coexistence of the TiO_2 HNPs and Au@Ag CSNPs (Supporting Information, Figure S2).

Characterization of the TiO_2 Hollow Nanoparticles. Figure 5a exhibits XRD patterns of the TiO_2 HNPs, together with those for commercially available P25, for comparison. The XRD patterns of TiO_2 HNPs exhibit peaks corresponding to the anatase phase, which has a larger electron diffusion coefficient than the rutile phase of TiO_2, which can lead to

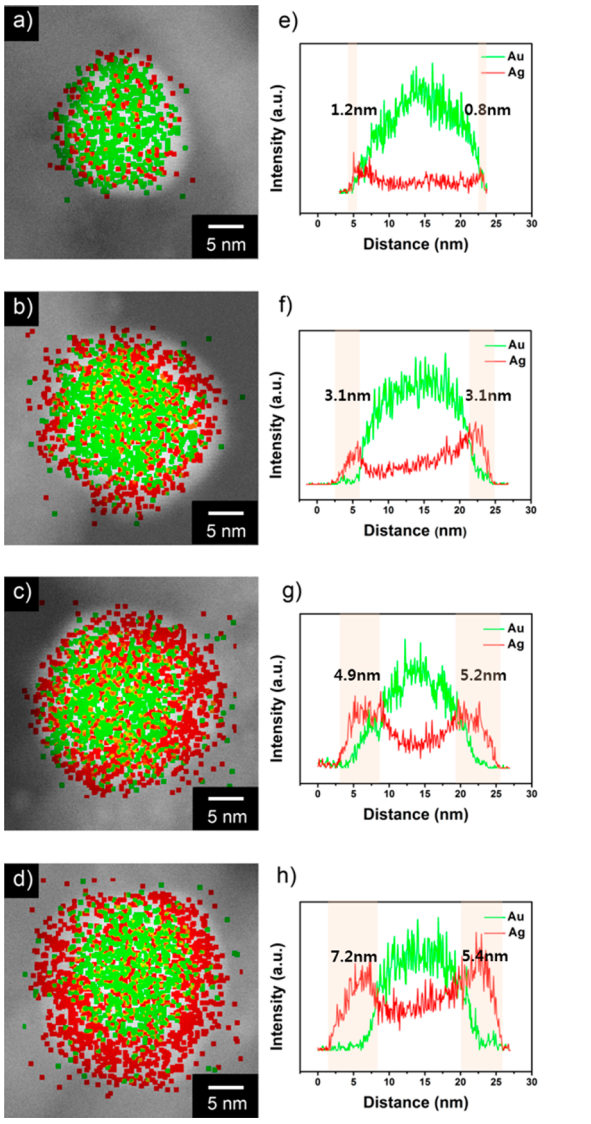

Figure 4. (a–d) EELS dot mappings and (e–f) STEM-EDS line mappings of S1–S4. The green color represents Au, while the red color represents Ag.

improved performance in DSSCs.[38] In the case of P25, the peaks in XRD analysis are consistent with the anatase and rutile phases, with an approximate ratio of 80:20. The inset of Figure 5a shows an HR-TEM image of the TiO_2 HNPs, which indicates a lattice constant of 0.35 nm in the [101] plane. Figure 5b shows N_2 adsorption–desorption isotherms together with a Brunauer–Emmett–Teller (BET) analysis of the data, and Figure 5c shows the equivalent Barrett–Joyner–Halenda (BJH) pore size distributions for the TiO_2 HNPs and P25. In contrast to P25, the TiO_2 HNPs show type IV isotherms, which is consistent with mesoporous characteristics and a large specific surface area.[39] The specific surface area of the TiO_2 HNPs was 129 $m^2\ g^{-1}$, and the specific surface area of P25 was 50 $m^2\ g^{-1}$. The TiO_2 HNPs had a significantly larger specific surface area than the P25 film had, which leads to improved dye loading in DSSCs. The sharp peaks in the BJH curves shown in Figure 5c for the TiO_2 HNPs indicate that these nanoparticles had pores with sizes of ~5 and ~35 nm. The smaller pores were distributed on the intrashell region of the TiO_2 HNPs, whereas the larger pores were located in the inner cavity of the

DOI: 10.1021/am508065n
ACS Appl. Mater. Interfaces 2015, 7, 2055–2063

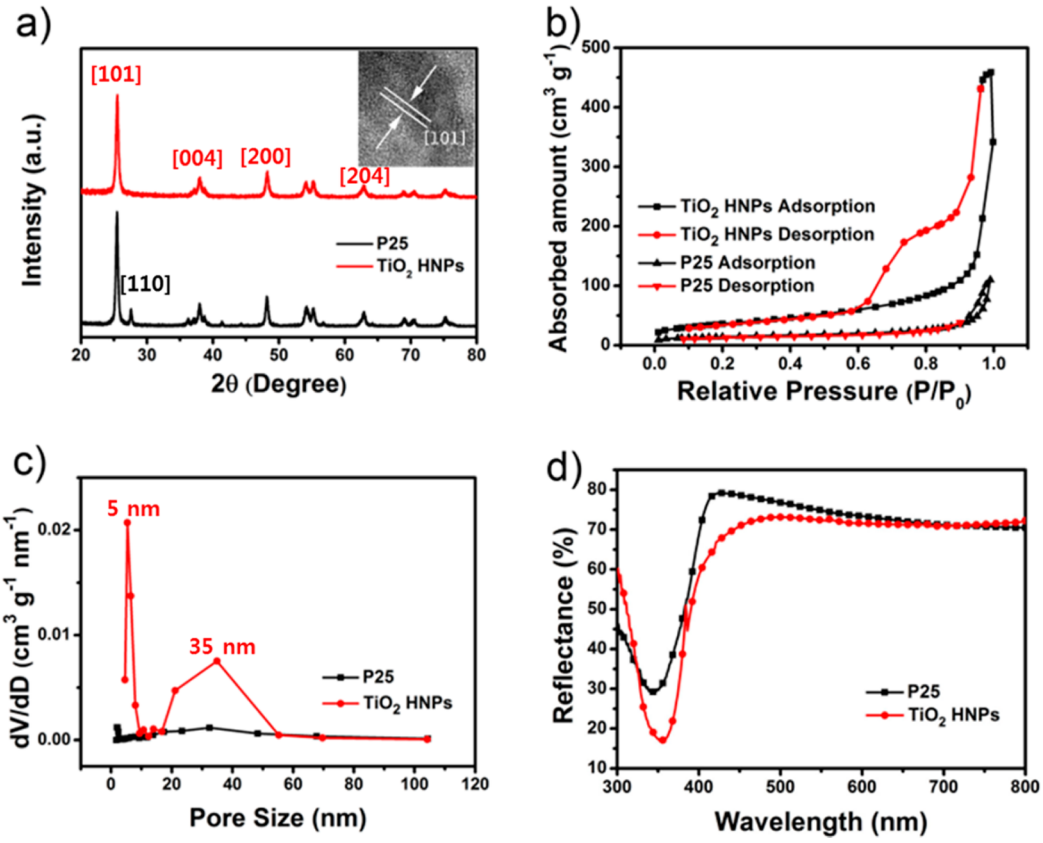

Figure 5. (a) XRD patterns of TiO_2 HNPs (red line) and P25 (black line). The inset of (a) is HR-TEM of TiO_2 HNPs. (b) BET analysis of TiO_2 HNPs (upper curve) and P25 (lower curve). (c) BJH pore size distribution and (d) DRS of TiO_2 HNPs (red line) and P25 (black line).

TiO_2 HNPs. The electrolyte can diffuse into the inner cavity via the intrashell pores, which results in facile oxidation−reduction reactions. Figure 5d displays diffuse reflectance spectra (DRS) of the TiO_2 HNPs and P25. The P25 exhibited light-scattering effects because the TiO_2 nanocrystals aggregate, which may effectively reflect visible light. The 100 nm diameter TiO_2 HNPs may also reflect the visible light via multiple scattering due to the hollow structure. Thus, both the TiO_2 HNPs and P25 can reflect visible light, enhancing light-harvesting properties. On the basis of these data, we can expect an increase in the optical scattering, a large dye-loading fraction, and favorable oxidation−reduction reactions of electrolyte.

The Optical Properties of Au@Ag/TiO_2 HNPs. Figure 6a shows UV/vis spectra of the TiO_2 HNPs with and without the Au, Ag, and Au@Ag CSNP nanoparticles to investigate the plasmonic characteristics. The TiO_2 HNPs exhibited an absorption edge at 350 nm, and the absorption of visible light was negligible. The Au/TiO_2 HNPs and Ag/TiO_2 HNPs exhibited plasmon bands with resonance peaks at 540 and 440 nm, respectively. The UV/vis spectra of the Au@Ag/TiO_2 HNPs exhibited two distinctive plasmon bands. The plasmonic characteristics of the Au core at 540 nm may be expected to be blue-shifted due to the presence of high-energy resonances that coincide with the resonance of the Ag nanoparticles near 440 nm.[26] As the thickness of the Ag shell increased, a blue-shift of the low-energy plasmon band occurred from 540 to 505 nm, as shown in Figure 6a. As the Ag shell became thicker, the blue-shifted low-energy plasmon band became weaker and converged to the resonance of the Ag nanoparticles due to blocking of the plasmon excitation of the Au core by the thick Ag shell. Compared with the Ag/TiO_2 HNPs, the S2/TiO_2 HNPs, although fabricated using the same total molarity of the precursor, exhibited a broader plasmon band with similar intensity. We may infer that the Au@Ag CSNPs have a synergetic effect in terms of the optical properties because of the interaction between the high-energy and low-energy plasmon bands. This synergetic effect cannot be considered as a linear combination of the individual contributions of Au core and Ag shell plasmon resonances and is instead attributed to an interaction between the core and the shell of Au@Ag CSNPs,[40] i.e., plasmon hybridization.[41] The increase in the amount of the Ag precursor did not significantly influence the form of spectra; however, according to Mie theory, it can be expected to result in stronger absorption owing to an increase in the size of the metal nanoparticles. Contrary to others, the absorption spectrum of S4 displays a slightly higher absorbance than that of S3, which is attributed to loss of Ag precursor, as described earlier. To investigate the effect of the composition of the nanoparticles on the absorption, we obtained UV/vis spectra of a mixed solution of ruthenium dye and samples, which were measured with an accurately controlled concentration (2.5×10^{-5} M) of the dye and of the nanoparticles (5×10^{-3} M), as shown in Figure 6b. The UV/vis spectra of the pure dye in ethanol (EtOH) exhibited two peaks, at 380 and 530 nm. When the dye solution was dispersed with the TiO_2 HNPs, the intensity of the peak at 380 nm increased due to absorption by the TiO_2 HNPs around 300 nm. The Au/TiO_2 HNPs and Ag/TiO_2 HNPs increased the absorption due to the LSPR of the Au and Ag nanoparticles. As the plasmon band became broader due to the presence of the Au@Ag CSNPs, the absorbance of the nanoparticle/dye dispersion was larger than that of Au/TiO_2 HNPs and Ag/TiO_2 HNPs. In particular, the

DOI: 10.1021/am508065n
ACS Appl. Mater. Interfaces 2015, 7, 2055−2063

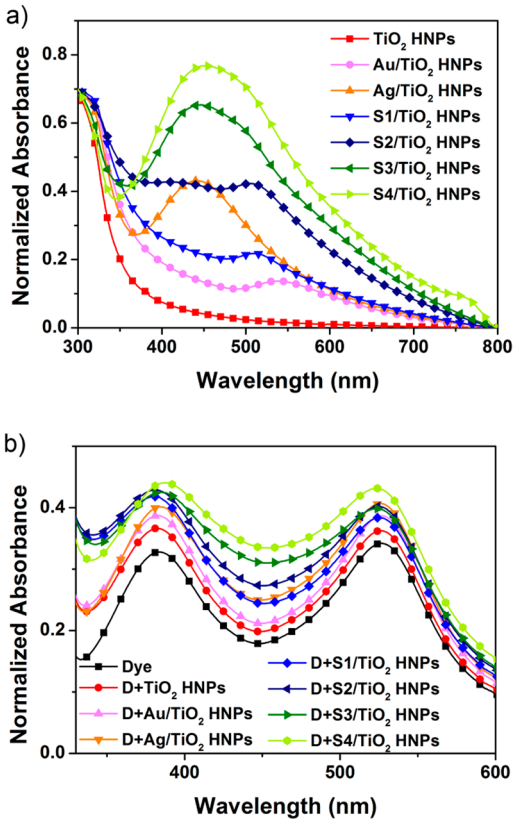

Figure 6. (a) UV/vis absorption spectra of the TiO_2 HNPs and metal nanoparticles-decorated TiO_2 HNPs (metal nanoparticles: Au, Ag, Au@Ag CSNPs). (b) Absorption spectra of the TiO_2 HNPs and metal nanoparticles-decorated TiO_2 HNPs with dye in EtOH.

S2/TiO_2 HNPs, which exhibited a similar intensity of the plasmon band and had the same molarity of Ag precursor as the Ag/TiO_2 HNPs, also exhibited an absorption coefficient that was significantly larger than that of the Ag/TiO_2 HNPs in the visible light region. The addition of metal nanoparticles to the dye solution can increase the efficiency of dye excitation or act as a sensitizer via coupling of the LSPR due to the metal nanoparticles and the photogeneration of electron−hole pairs in the TiO_2 HNPs.[42] On the basis of these data, we may infer that the introduction of the Ag shell caused the plasmon band to exhibit stronger and broader absorption, which can be expected to increase the photocurrent in DSSCs.

Effect of Hollow Structure and LSPR of Au@Ag/TiO_2 HNPs on DSSCs. Figure 7a shows a schematic diagram of the structure of a DSSC incorporating Au@Ag/TiO_2 HNPs. The photoanode film consists of dye-adsorbed TiO_2 HNPs and Au@Ag/TiO_2 HNPs. Figure 7b shows a magnified image of the Au@Ag/TiO_2 HNPs, indicating the LSPR, multiple scattering, and large specific surface area. These properties can be expected to improve the light-harvesting properties.

To investigate the effects of the Au@Ag/TiO_2 HNPs coated with SiO_2 on the performance of DSSCs, we controlled the film thickness and the ratio of the metal nanoparticles to the TiO_2 HNPs. The power conversion efficiency (PCE) of all samples was averaged after 15 experiments under the same conditions. All PCE in this paper were averaged by repeated experiments to provide the evidence for the improvement. To prevent corrosion of the Au@Ag CSNPs due to the iodide electrolyte in the DSSCs, a thin passivation layer of SiO_2 was coated onto the Au@Ag/TiO_2 HNPs using the Stöber method (Supporting Information, Figure S3).[33] The introduction thin layer of SiO_2 led to a red-shift of the plasmon band, as shown in Supporting Information, Figure S4. This small red-shift of LSPR band is caused by the reflective index of SiO_2 shell. In the case of metal core particles smaller than 30 nm, the LSPR band mostly is affected by the refractive index of the SiO_2 shell, accompanied by a red-shift owing to presence of multipole effects.[43] To examine the effects of the TiO_2 HNPs in DSSCs, we compared the performance of DSSCs based on TiO_2 HNPs with that of DSSCs based on P25. The DSSCs based on TiO_2 HNPs exhibited an enhanced photocurrent density of J_{sc} = 15.8 mA cm^{-2} and power conversion efficiency (PCE) of η = 8.3%; this is an improvement on the metrics for P25, where we find J_{sc} = 14.1 mA cm^{-2} and η = 7.8%, as shown in Figure 8a,b and listed in Table 1. Supporting Information, Figure S7 shows the histogram displaying the distribution of PCE of each sample in Table 1. The DSSCs based on TiO_2 HNPs exhibited improved PCE due to the larger specific surface area, multiple scattering effects, and improved oxidation−reduction of the electrolyte due to the hollow structure. UV/vis spectra of dye solution desorbed from each film are shown in Supporting Information, Figure S5a. The large absorption means that the film has a large specific surface area. The film based on the TiO_2 HNPs exhibited a larger specific surface area than that of the P25. Additionally, to investigate the LSPR effect of the Au@Ag

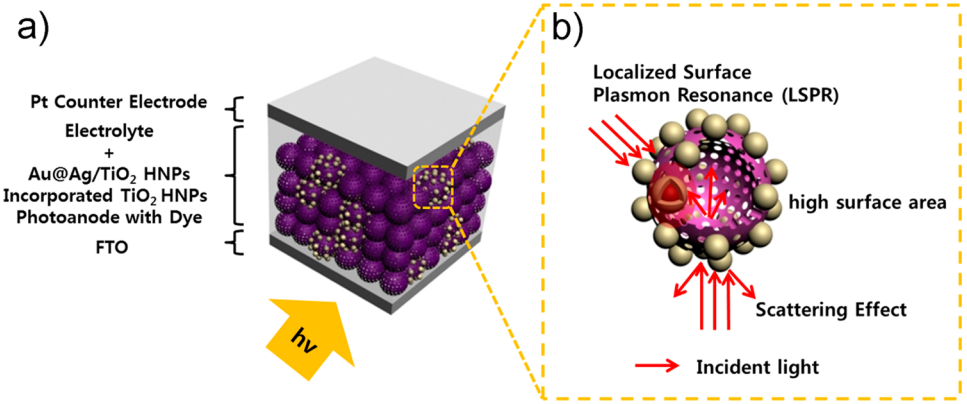

Figure 7. (a) Schematic illustration of Au@Ag/TiO_2 HNPs-incorporated photoanode in TiO_2 HNPs-based DSSC. (b) A magnified structure of an Au@Ag/TiO_2 HNPs.

DOI: 10.1021/am508065n
ACS Appl. Mater. Interfaces 2015, 7, 2055−2063

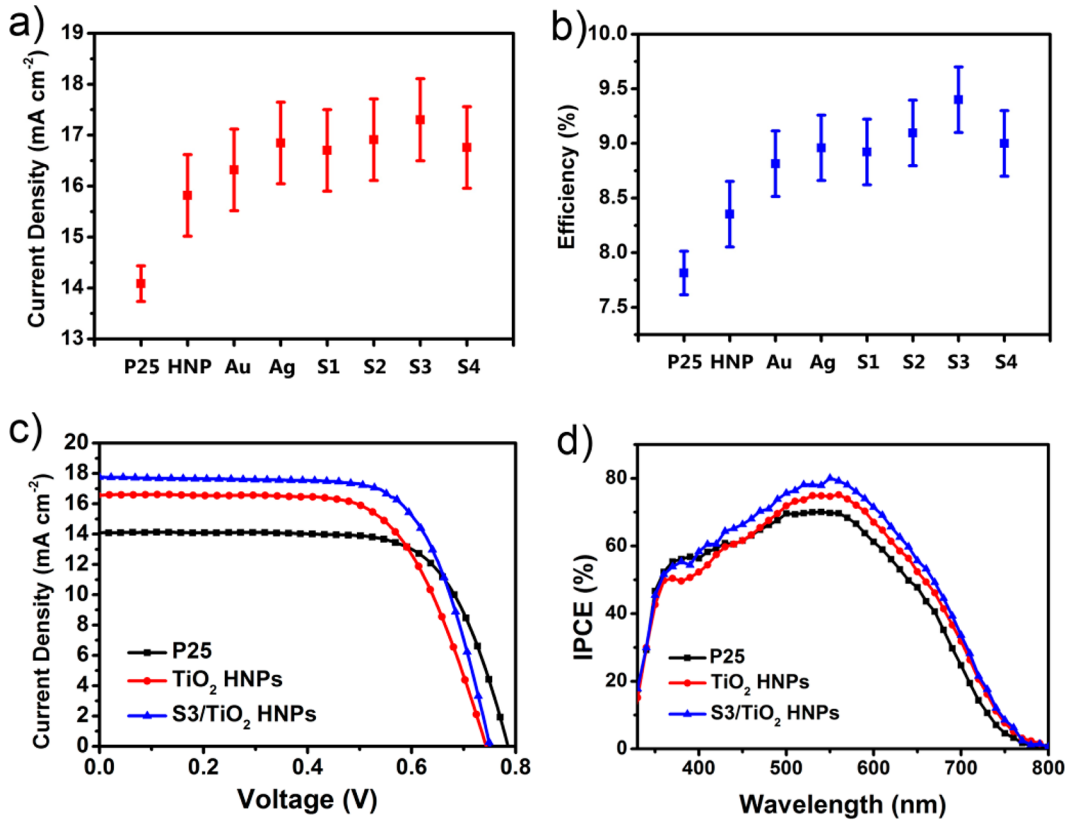

Figure 8. (a) Short-circuit current and (b) PCE of DSSCs using P25, TiO_2 HNPs, and blend of TiO_2 HNPs and metal nanoparticles-decorated TiO_2 HNPs (0.2 wt % metal nanoparticles with respect to TiO_2 HNPs). (c) Representative $J-V$ curves and (d) IPCE spectra for P25, TiO_2 HNPs and TiO_2 HNPs incorporating S3/TiO_2 HNPs (0.2 wt % Au@Ag CSNPs with respect to TiO_2 HNPs).

Table 1. Photovoltaic Parameter Based on TiO_2 HNPs Photoanodes with and without Au@Ag/TiO_2 HNPs Coated with a SiO_2 Layer

sample[a]	J_{sc}[b] (mA cm^{-2})	V_{oc}[c] (V)	FF[d]	η[e] (%)
P25	14.1	0.79	0.71	7.8
TiO_2 HNP	15.8	0.74	0.71	8.3
Au/TiO_2 HNP	16.3	0.75	0.72	8.8
Ag/TiO_2 HNP	16.8	0.75	0.71	9.0
S1/TiO_2 HNP	16.7	0.75	0.71	8.8
S2/TiO_2 HNP	16.9	0.75	0.72	9.1
S3/TiO_2 HNP	17.3	0.75	0.72	9.4
S4/TiO_2 HNP	16.8	0.75	0.71	9.0

[a]Active area of the assembled DSSC samples is 0.16 cm^2. [b]Short-circuit current. [c]Open-circuit voltage. [d]Fill factor. [e]Power conversion efficiency.

CSNPs on the performance of DSSCs, we examined the S3/TiO_2 HNPs, which exhibited a particularly strong plasmon band and negligible loss of the Ag precursor. We prepared a TiO_2 HNPs film using the S3 HNPs with content in the range 0−0.4 wt % to determine the optimum conditions. The amount of Au@Ag CSNPs was calculated from the ratio of the quantity precursor used to form the Au seed to that used to form the Ag shell, assuming that all of the precursors reacted. The efficiency is indicated by the current−voltage ($J-V$) curves shown in Supporting Information, Figure S6a and the data listed in Supporting Information, Table S1. The histogram statistics related to PCE of each condition was shown in Supporting Information, Figure S8. The PCE and current density of the DSSCs increased as the amount of Au@Ag CSNPs increased up to 0.2 wt % and decreased with larger fractions on the Au@Ag nanoparticles. An excess of the Au@Ag CSNPs may lead to increased trapping of photogenerated electrons as well as increased optical absorption, which may convert part of the incident energy to heat.[44] The open circuit voltage (V_{oc}) also slightly increased with the addition of silica coated Au@Ag/TiO_2 HNPs because a small quantity of insulating silica thin layer on Au@Ag/TiO_2 HNPs functions as retarding electron recombination at photoanode interfaces.[45] To further investigate the effects of the LSPR, we fixed the concentration of nanoparticles at 0.2 wt %. Figure 8a shows the photocurrent density, and Figure 8b shows the PCE of each of the DSSCs based on each of the samples. The $J-V$ curves are also shown for each of the samples in Supporting Information, Figure S6b. The DSSCs formed using Au/TiO_2 and Ag/TiO_2 exhibited larger PCE and current densities than did those based on Au/TiO_2 HNPs. This is attributed to the stronger intensity of the plasmon bands for the Ag nanoparticles compared with the Au nanoparticles. DSSCs formed using Au@Ag/TiO_2 HNPs exhibited photocurrent density and PCE that increased from samples S1 to S3 and then decreased for sample S4. The DSSC based on S3/TiO_2 exhibited the largest photocurrent density and PCE due to the intense and broad plasmon band. Sample S4 had the highest intensity plasmon band; however, this enhanced optical absorption may result in part of the solar energy being lost as heat. Furthermore, aggregation of metal nanoparticles could lead to a reduction in plasmonic activity. Supporting Information, Figure S5b shows absorption spectra of the dye solution desorbed from the film with and without the S3/TiO_2 HNPs. These data suggest that the presence of Au@

DOI: 10.1021/am508065n
ACS Appl. Mater. Interfaces 2015, 7, 2055−2063

Ag CSNPs in the film does not significantly affect the dye loading. Thus, the enhanced efficiency of the Au@Ag CSNPs is attributed to surface plasmon resonance. DSSCs based on the S3/TiO_2 HNPs exhibited photocurrent density of J_{sc} = 17.3 mA cm^{-2} and PCE of η = 9.4%, which are larger values than those for the DSSCs based on TiO_2 HNPs, where J_{sc} = 15.8 mA cm^{-2} and η = 8.3%. Figure 8c shows representative $J-V$ curves for DSSCs based on P25, TiO_2 HNPs, and S3/TiO_2 HNPs. These data help us to gain insight into the above-mentioned effects. The incident photon-to-electron conversion efficiency (IPCE) is shown in Figure 8d. The increased specific surface area of the TiO_2 HNPs increased the quantum efficiency at wavelengths in the range 400−800 nm. At wavelengths shorter than 400 nm, the DSSCs based on P25 exhibited increased quantum efficiency, which is attributed to more effective light scattering. Furthermore, the tuned LSPR effect of the Au@Ag CSNPs enhanced the quantum efficiency at wavelengths in the range 350−650 nm. These results suggest that the S3/TiO_2 HNPs are promising photoanode materials for DSSCs applications because of larger specific surface area, favorable optical scattering, facile oxidation−reduction profiles of the electrolyte, and the strong and broad LSPR.

By exploiting the large specific surface area, optical scattering, facile oxidation−reduction of the electrolyte, and strong LSPR of the Au@Ag/TiO_2 HNPs, we may further enhance the PCE of DSSCs. Figure 9 shows a $J-V$ curve of a DSSC based on S3/TiO_2 HNPs. We find J_{sc} = 18.2 mA cm^{-2}, V_{oc} = 0.754 V, FF = 71%, and PCE of η = 9.7%, with an irradiance under 1.5 G, i.e., solar light intensity. This value of PCE was 24% larger than the PCE of the DSSC based on P25.

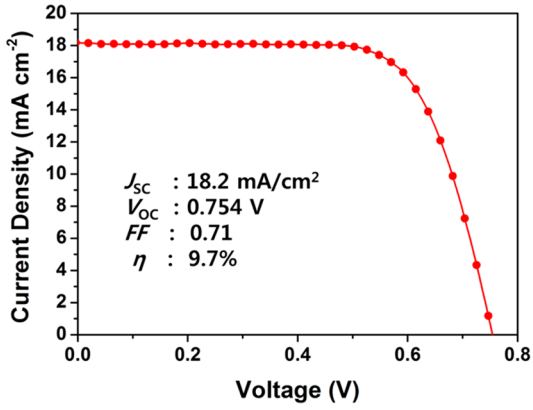

Figure 9. Current−voltage curve of best performing DSSCs based on S3/TiO_2 HNPs.

CONCLUSIONS

We have described the fabrication of Au@Ag/TiO_2 HNPs via sol−gel coating and chemical deposition. The Au@Ag CSNPs exhibited stronger and broader surface plasmon resonance than either the Au or Ag nanoparticles. By varying the thickness of the Ag shell, we were able to control the LSPR and to investigate the interaction between the Au core and Ag shell. TiO_2 HNPs with a larger specific surface area provide sufficient dye loading and effective optical scattering, leading to increased PCE compared with using P25 nanoparticles. The overall PCE of η = 9.7% was achieved by incorporating the Au@Ag/TiO_2 HNPs into the photoanode material for the DSSCs, which is a significant improvement compared with DSSCs formed using P25, where we find η = 7.8%. The approach described here enables the fabrication of novel structured Au@Ag/TiO_2 HNPs with a large specific surface area, large optical scattering effect, and tuned LSPR. The applications of these nanoparticles extend beyond DSSCs to include photocatalysis, perovskite solar cells, organic solar cells, and antimicrobial therapy.

EXPERIMENTAL SECTION

Materials. Titanium(IV) isopropoxide (TIP, 97%), titanium(IV) chloride ($TiCl_4$, 99%), tetraethylorthosilicate (TEOS, 98%), sodium hydroxide (NaOH, 99%), silver nitrate ($AgNO_3$, 99%), gold chloride ($AuCl_3$, 99%), 3-mercapto-propyltrimethoxysilane (MPTS, 98%), and polyvinylpyrrolidone (PVP, MW = 55000) were obtained from Aldrich Chemical Co. (St. Louis, MO). Ammonia solution (28−32.4%) was purchased from Samchun Chemical Co. P25, *cis*-disothiocyanato-bis(2,20-bipyridyl-4,40-dicarboxylato)ruthenium-(II) bis(tetrabutylammonium) (N 719), 1-butyl-3-methyl-imidazolium iodide (BMII), lithium iodide (LiI), and iodine (I_2) were purchased from Solaronix (Aubonne, Switzerland). FTO glass (15Ω cm^{-2}, thickness of 2.2 mm) was purchased from Pilkington (Toledo, USA)

Synthesis of TiO_2 Hollow Nanoparticles. The synthesis of the TiO_2 HNPs began with a colloidal dispersion of SiO_2 nanoparticles (0.75 g) prepared according to the Stöber method.[33] Titanium isopropoxide (TIP, 3.6 mL) was then injected in a solution with 18 mL of ethanol and 6 mL of acetonitrile. The TIP solution reacted with the SiO_2 nanoparticles via a sol−gel coating process for 6 h at 4 °C. The SiO_2@TiO_2 CSNPs were then isolated via centrifugation and washed with ethanol and DI water. The resulting SiO_2@TiO_2 CSNPs, weighing 1.7 g and with 42% yield, were calcinated at 900 °C for 6 h and then redispersed in 20 mL of DI water. TiO_2 HNPs were obtained via selective removal of the SiO_2 core by adding an aqueous solution of NaOH (2.5 M, 4 mL) to the redispersed solution and stirring for 6 h. Following etching, the resulting TiO_2 HNPs, weighing 0.9 g and with 52% yield, were separated by centrifugation and then washed with ethanol and DI water.

Synthesis of Au@Ag/TiO_2 HNPs. Thiol-functionalized surfaces of TiO_2 HNPs were obtained by dispersing 100 mg of the TiO_2 HNPs in 10 mL of ethanol via sonication. Then, 20 μL of 3-mercapto-propyltrimethoxysilane (MPTS) and 50 μL of 28−32.4 wt % aqueous ammonia solution were added to the TiO_2 HNPs suspension. The solution was stirred using a magnetic bar for 12 h. The MPTS-treated TiO_2 HNPs were isolated by centrifugation and washed with ethanol. To decorate the TiO_2 HNPs with Au nanoparticles, 100 mg of the MPTS-treated TiO_2 HNPs was dispersed uniformly in 100 mL of ethylene glycol, followed by the addition of 45 mg of gold chloride (in case of Ag/TiO_2 HNPs; 50 mg silver nitrate) and 350 mg of polyvinylpyrrolidone (PVP) with a molecular weight of M_w = 55000. Octylamine (OA, 200 μL) was rapidly injected into the mixed solution at 90 °C as reduction agent, and the mixture was allowed to react for 3 h. Then the Au/TiO_2 HNPs, weighing 129 mg and with 88% yield, were washed with ethanol. To form the Ag shell coating, the Au/TiO_2 HNPs were redispersed in 100 mL of ethylene glycol and 350 mg of PVP was added, together with a systematically varied quantity of silver nitrate. Then, 100 μL of OA was rapidly injected into the mixed solution at 90 °C and allowed to react for 3 h. The Au@Ag/TiO_2 HNPs, weighing 145 mg and with 82% yield in the case of S3/TiO_2 HNPs, were isolated by centrifugation, washed with ethanol and DI water, and dried in a vacuum oven.

Fabrication of Au@Ag/TiO_2 HNPs with SiO_2 Passivation Layer. The Au@Ag/TiO_2 HNPs (100 mg) were redispersed in 10 mL of DI water together with 100 mg of PVP and stirred overnight to allow adsorption onto the surface of the Au@Ag/TiO_2 HNPs. The PVP-treated Au@Ag/TiO_2 HNPs were then centrifuged, washed, and redispersed in 7.9 mL of ethanol. The colloidal dispersion was then mixed with 1.4 mL of DI water, 3.9 mL of ammonia solution, and 50 μL of tetraethyl orthosilicate, stirred at 38 °C for 4 h, centrifuged, washed, and dried in a vacuum oven.

Assembly of Dye-Sensitized Solar Cells. To assemble the photoanode film, pastes were prepared from the P25 and TiO_2 HNPs

DOI: 10.1021/am508065n
ACS Appl. Mater. Interfaces 2015, 7, 2055−2063

with and without metal nanoparticles. A fluorine-doped tin oxide (FTO) glass substrate was washed using DI water, acetone, and 2-propanol and then treated with 40 mM aqueous $TiCl_4$ solution and calcinated at 450 °C for 30 min. Photoanodes of 10 μm thickness were prepared via screen-printing, heated at 450 °C for 30 min, treated with $TiCl_4$ solution, and then calcinated again under the same conditions. The photoanode films were then immersed in an ethanol-based dye solution (N719, 5×10^{-4} M) and kept at room temperature for 18 h. The counter electrodes were prepared on the FTO glass by dropping 5 mM 2-propanol Pt (H_2PtCl_6) solution and then sintered at 400 °C for 30 min. The photoanodes were assembled with the Pt−FTO counter electrodes into sandwich-type cells using thermal adhesive films (Surlyn, 60 μm, Dupont). The electrolyte in the sealed cell was an I^-/I^{3-} redox couple consisting of 0.6 M 1-butyl-3-methyl-imidazolium iodide (BMII), 0.1 M LiI, 0.05 M I_2, and 0.5 M *tert*-butylpyridine in acetonitrile.

Characterization. The transmission electron microscopy (TEM) images and energy dispersive spectroscopy (EDS) analysis data of nanomaterials were obtained using a JEOL JEM-200CX and JEOL JSM 6700-F. The electron energy loss spectroscopy (EELS) mapping and scanning TEM/energy dispersive spectroscopy (STEM/EDS) line analysis data were taken with a JEOL JEM-2100F. X-ray diffraction measurements were carried out using an M18XHF-SRA (Mac Science Co., Yokohama, Japan) with a Cu Kα radiation source (λ = 1.5406 Å) at 40 kV and 300 mA (12 W). Brunauer−Emmett−Teller (BET) surface areas of TiO_2 HNPs were measured using a Micrometics analyzer (ASAP 2000; Micrometics Co., Norcross, GA). The UV/vis diffuse reflectance spectra (DRS) and UV/vis aborption spectra were determined by A Lambda (PerkinElmer). The photocurrent−voltage characteristics of the assembled DSSCs were investigated by 500 W xenon lamp (XIL model 05A50KS source units). The incident phototocurrent efficiency (IPCE; PV measurement, Inc., Boulder, CO) was obtained from 300 to 800 nm under the global AM 1.5 solar emission spectrum.

■ ASSOCIATED CONTENT

Ⓢ Supporting Information

TEM images of Au/TiO_2 HNPs and Ag/TiO_2 HNPs, EDS spectra of Au@Ag/TiO_2 HNPs, TEM images of silica coated Au@Ag/TiO_2 HNPs, UV−vis spectra of Au@Ag/TiO_2 HNPs with and without silica shell, absorption spectra of dye desorption from photo anode, current−voltage curve, and table for additional photovoltaic parameters. This material is available free of charge via the Internet at http://pubs.acs.org.

■ AUTHOR INFORMATION

Corresponding Author

*E-mail: jsjang@plaza.snu.ac.kr.

Notes

The authors declare no competing financial interest.

■ ACKNOWLEDGMENTS

This work was supported by Global Frontier R&D Program on Center for Multiscale Energy System funded by the National Research Foundation under the Ministry of Education, Science and Technology, Korea (2011-0031573).

■ REFERENCES

(1) O'Regan, B.; Grätzel, M. A Low-Cost, High-Efficiency Solar Cell Based on Dye-Sensitized Colloidal TiO2 Films. *Nature* **1991**, *353*, 737−740.

(2) Grätzel, M. Photoelectrochemical Cells. *Nature* **2001**, *414*, 338−344.

(3) Hagfeldt, A.; Boschloo, G.; Sun, L.; Kloo, L.; Pettersson, H. Dye-Sensitized Solar Cells. *Chem. Rev.* **2010**, *110*, 6595−6663.

(4) Yella, A.; Lee, H. W.; Tsao, H. N.; Yi, C.; Chandiran, A. K.; Nazeeruddin, M. K.; Diau, E. W. G.; Yeh, C. Y.; Zakeeruddin, S. M.; Grätzel, M. Porphyrin-Sensitized Solar Cells with Cobalt (II/III)-Based Redox Electrolyte Exceed 12% Efficiency. *Science* **2011**, *334*, 629−634.

(5) Chandiran, A. K.; Comte, P.; Humphry-Baker, R.; Kessler, F.; Yi, C.; Nazeeruddin, M. K.; Grätzel, M. Evaluating The Critical Thickness of TiO_2 Layer on Insulating Mesoporous Templates for Efficient Current Collection in Dye-Sensitized Solar Cells. *Adv. Funct. Mater.* **2013**, *23*, 2775−2781.

(6) Standridge, S. D.; Schatz, G. C.; Hupp, J. T. Distance Dependence of Plasmon-Enhanced Photocurrent in Dye-Sensitized Solar Cells. *J. Am. Chem. Soc.* **2009**, *131*, 8407−8409.

(7) Standridge, S. D.; Schatz, G. C.; Hupp, J. T. Toward Plasmonic Solar Cells: Protection of Silver Nanoparticles via Atomic Layer Deposition of TiO_2. *Langmuir* **2009**, *25*, 2596−2600.

(8) Jeong, N. C.; Prasittichai, C.; Hupp, J. T. Photocurrent Enhancement by Surface Plasmon Resonance of Silver Nanoparticles in Highly Porous Dye-Sensitized Solar Cells. *Langmuir* **2011**, *27*, 14609−14614.

(9) Brown, M. D.; Suteewong, T.; Kumar, R. S. S.; D'Innocenzo, V.; Petrozza, A.; Lee, M. M.; Wiesner, U.; Snaith, H. J. Plasmonic Dye-Sensitized Solar Cells Using Core−Shell Metal-Insulator Nanoparticles. *Nano Lett.* **2011**, *11*, 438−445.

(10) Rühle, S.; Shalom, M.; Zaban, A. Quantum-Dot-Sensitized Solar Cells. *ChemPhysChem* **2010**, *11*, 2290−2304.

(11) Lee, E.; Ryu, J.; Jang, J. Fabrication of Graphene Quantum Dots via Size-Selective Precipitation and Their Application in Upconversion-Based DSSCs. *Chem. Commun.* **2013**, *49*, 9995−9997.

(12) Jeong, N. C.; Farha, O. K.; Hupp, J. T. A Convenient Route to High Area, Nanoparticulate TiO_2 Photoelectrodes Suitable for High-Efficiency Energy Conversion in Dye-Sensitized Solar Cells. *Langmuir* **2011**, *27*, 1996−1999.

(13) Jeong, N. C.; Son, H. J.; Prasittichai, C.; Lee, C. Y.; Jensen, R. A.; Farha, O. K.; Hupp, J. T. Effective Panchromatic Sensitization of Electrochemical Solar Cells: Strategy and Organizational Rules for Spatial Separation of Complementary Light Harvesters on High-Area Photoelectrodes. *J. Am. Chem. Soc.* **2012**, *134*, 19820−19827.

(14) Son, S.; Hwang, S. H.; Kim, C.; Yun, J. Y.; Jang, J. Designed Synthesis of SiO_2/TiO_2 Core/Shell Structure as Light Scattering Material for Highly Efficient Dye-Sensitized Solar Cells. *ACS Appl. Mater. Interfaces* **2013**, *5*, 4815−4820.

(15) Hore, S.; Vetter, C.; Kern, R.; Smit, H.; Hinsch, A. Influence of Scattering Layers on Efficiency of Dye-Sensitized Solar Cells. *Sol. Energy Mater. Sol. Cells* **2006**, *90*, 1176−1188.

(16) Ferber, J.; Luther, J. Computer Simulations of Light Scattering and Absorption in Dye-Sensitized Solar Cells. *Sol. Energy Mater. Sol. Cells* **1998**, *54*, 265−275.

(17) Law, M.; Greene, L. E.; Johnson, J. C.; Saykally, R.; Yang, P. Nanowire Dye-Sensitized Solar Cells. *Nature Mater.* **2005**, *4*, 455−459.

(18) Shankar, K.; Basham, J. I.; Allam, N. K.; Varghese, O. K.; Mor, G. K.; Feng, X.; Paulose, M.; Seabold, J. A.; Choi, K. S.; Grimes, C. A. Recent Advances In the Use of TiO_2 Nanotube and Nanowire Arrays for Oxidative Photoelectrochemistry. *J. Phys. Chem. C* **2009**, *113*, 6327−6359.

(19) Mor, G. K.; Shankar, K.; Paulose, M.; Varghese, O. K.; Grimes, C. A. Use of Highly-Ordered TiO_2 Nanotube Arrays in Dye-Sensitized Solar Cells. *Nano Lett.* **2006**, *6*, 215−218.

(20) Brown, P.; Takechi, K.; Kamat, P. V. Single-Walled Carbon Nanotube Scaffolds for Dye-Sensitized Solar Cells. *J. Phys. Chem. C* **2008**, *112*, 4776−4782.

(21) Tang, Y. B.; Lee, C. S.; Xu, J.; Liu, Z. T.; Chen, Z. H.; He, Z.; Cao, Y. L.; Yuan, G.; Song, H.; Chen, L.; Luo, L.; Cheng, H. M.; Zhang, W. J.; Bello, I.; Lee, S. T. Incorporation of Graphenes in Nanostructured TiO_2 Films via Molecular Grafting for Dye-Sensitized Solar Cell Application. *ACS Nano* **2010**, *4*, 3482−3488.

(22) Choi, H.; Chen, W. T.; Kamat, P. V. Know thy Nano Neighbor. Plasmonic Versus Electron Charging Effects of Metal Nanoparticles in Dye-Sensitized Solar Cells. *ACS Nano* **2012**, *6*, 4418−4427.

DOI: 10.1021/am508065n
ACS Appl. Mater. Interfaces 2015, 7, 2055−2063

(23) Banerjee, M.; Sharma, S.; Chattopadhyay, A.; Ghosh, S. S. Enhanced Antibacterial Activity of Bimetallic Gold−Silver Core−Shell Nanoparticles at Low Silver Concentration. *Nanoscale* **2011**, *3*, 5120−5125.
(24) Millstone, J. E.; Métraux, G. S.; Mirkin, C. A. Controlling the Edge Length of Gold Nanoprisms via a Seed-Mediated Approach. *Adv. Funct. Mater.* **2006**, *16*, 1209−1214.
(25) Niu, W.; Zheng, S.; Wang, D.; Liu, X.; Li, H.; Han, S.; Chen, J.; Tang, Z.; Xu, G. Selective Synthesis of Single-Crystalline Rhombic Dodecahedral, Octahedral, and Cubic Gold Nanocrystals. *J. Am. Chem. Soc.* **2009**, *131*, 697−703.
(26) Chuntonov, L.; Bar-Sadan, M.; Houben, L.; Haran, G. Correlating Electron Tomography and Plasmon Spectroscopy of Single Noble Metal Core−Shell Nanoparticles. *Nano Lett.* **2012**, *12*, 145−150.
(27) Gonzalez, C. M.; Liu, Y.; Scaiano, J. C. Photochemical Strategies for the Facile Synthesis of Gold−Silver Alloy and Core−Shell Bimetallic Nanoparticles. *J. Phys. Chem. C* **2009**, *113*, 11861−11867.
(28) Zhang, X.; Su, Z. Polyelectrolyte-Multilayer-Supported Au@Ag Core−Shell Nanoparticles with High Catalytic Activity. *Adv. Mater.* **2012**, *24*, 4574−4577.
(29) Ito, S.; Murakami, T. N.; Comte, P.; Liska, P.; Grätzel, C.; Nazeeruddin, M. K.; Grätzel, M. Fabrication of Thin Film Dye Sensitized Solar Cells with Solar to Electric Power Conversion Efficiency over 10%. *Thin Solid Films* **2008**, *516*, 4613−4619.
(30) Zhu, K.; Neale, N. R.; Miedaner, A.; Frank, A. J. Enhanced Charge-Collection Efficiencies and Light Scattering in Dye-Sensitized Solar Cells Using Oriented TiO_2 Nanotubes Arrays. *Nano Lett.* **2007**, *7*, 69−74.
(31) Koo, H. J.; Kim, Y. J.; Lee, Y. H.; Lee, W. I.; Kim, K.; Park, N. G. Nano-Embossed Hollow Spherical TiO_2 as Bifunctional Material for High-Efficiency Dye-Sensitized Solar Cells. *Adv. Mater.* **2008**, *20*, 195−199.
(32) Hwang, S. H.; Kim, C.; Song, H.; Son, S.; Jang, J. Designed Architecture of Multiscale Porous TiO_2 Nanofibers for Dye-Sensitized Solar Cells Photoanode. *ACS Appl. Mater. Interfaces* **2012**, *4*, 5287−5292.
(33) Hwang, S. H.; Shin, D. H.; Yun, J.; Kim, C.; Choi, M.; Jang, J. SiO_2/TiO_2 Hollow Nanoparticles Decorated with Ag Nanoparticles: Enhanced Visible Light Absorption and Improved Light Scattering in Dye-Sensitized Solar Cells. *Chem.—Eur. J.* **2014**, *20*, 4439−4446.
(34) Chen, D.; Huang, F.; Cheng, Y. B.; Caruso, R. A. Mesoporous Anatase TiO_2 Beads with High Surface Areas and Controllable Pore Sizes: A Superior Candidate for High-Performance Dye-Sensitized Solar Cells. *Adv. Mater.* **2009**, *21*, 2206−2210.
(35) Choi, M.; Kim, C.; Jeon, S. O.; Yook, K. S.; Lee, J. Y.; Jang, J. Synthesis of Titania Embedded Silica Hollow Nanospheres via Sonication Mediated Etching and Re-deposition. *Chem. Commun.* **2011**, *47*, 7092−7094.
(36) Kim, J. H.; Kim, J. S.; Choi, H.; Lee, S. M.; Jun, B. H.; Yu, K. N.; Kuk, E.; Kim, Y. K.; Jeong, D. H.; Cho, M. H.; Lee, Y. S. Nanoparticle Probes with Surface Enhanced Raman Spectroscopic Tags for Cellular Cancer Targeting. *Anal. Chem.* **2006**, *78*, 6967−6973.
(37) Ma, Y.; Li, W.; Cho, E. C.; Li, Z.; Yu, T.; Zeng, J.; Xie, Z.; Xia, Y. Au@Ag Core−Shell Nanocubes with Finely Tuned and Well-Controlled Sizes, Shell Thicknesses, and Optical Properties. *ACS Nano* **2010**, *4*, 6725−6734.
(38) Park, N. G.; Van De Lagemaat, J.; Frank, A. J. Comparison of Dye-Sensitized Rutile- and Anatase-Based TiO_2 Solar Cells. *J. Phys. Chem. B* **2000**, *104*, 8989−8994.
(39) Joo, J. B.; Lee, I.; Dahl, M.; Moon, G. D.; Zaera, F.; Yin, Y. Controllable Synthesis of Mesoporous TiO_2 Hollow Shells: Toward an Efficient Photocatalyst. *Adv. Funct. Mater.* **2013**, *23*, 4246−4254.
(40) Zhang, X.; Wang, H.; Su, Z. Fabrication of Au@Ag Core−Shell Nanoparticles Using Polyelectrolyte Multilayers as Nanoreactors. *Langmuir* **2012**, *28*, 15705−15712.
(41) Prodan, E.; Radloff, C.; Halas, N. J.; Nordlander, P. A Hybridization Model for the Plasmon Response of Complex Nanostructures. *Science* **2003**, *302*, 419−422.
(42) Evanoff, D. D., Jr; Chumanov, G. Synthesis and Optical Properties of Silver Nanoparticles and Arrays. *ChemPhysChem* **2005**, *6*, 1221−1231.
(43) Baida, H.; Billaud, P.; Marhaba, S.; Christofilos, D.; Cottancin, E.; Crut, A.; Lermé, J.; Maioli, P.; Pellarin, M.; Broyer, M.; Del Fatti, N.; Vallée, F.; Sánchez-Iglesias, A.; Pastoriza-Santos, I.; Liz-Marzán, L. M. Quantitative Determination of the Size Dependence of Surface Plasmon Resonance Damping in Single $Ag@SiO_2$ Nanoparticles. *Nano Lett.* **2009**, *9*, 3463−3469.
(44) Qi, J.; Dang, X.; Hammond, P. T.; Belcher, A. M. Highly Efficient Plasmon-Enhanced Dye-Sensitized Solar Cells through Metal@oxide Core−Shell Nanostructure. *ACS Nano* **2011**, *5*, 7108−7116.
(45) Son, H. J.; Wang, X.; Prasittichai, C.; Jeong, N. C.; Aaltonen, T.; Gordon, R. G.; Hupp, J. T. Glass-Encapsulated Light Harvesters: More Efficient Dye-Sensitized Solar Cells by Deposition of Self-aligned, Conformal, and Self-Limited Silica Layers. *J. Am. Chem. Soc.* **2012**, *134*, 9537−9540.

DOI: 10.1021/am508065n
ACS Appl. Mater. Interfaces 2015, 7, 2055−2063